Reversible high-pressure carbon nanotube vessel

Citation: Ma, Ming D. et al. "Reversible high-pressure carbon nanotube vessel." Physical Review B 81.23 (2010): 235420. © 2010 The American Physical Society.

As Published: http://dx.doi.org/10.1103/PhysRevB.81.235420

Publisher: American Physical Society

Persistent URL: http://hdl.handle.net/1721.1/60909

Version: Final published version: final published article, as it appeared in a journal, conference proceedings, or other formally published context

Reversible high-pressure carbon nanotube vessel

Ming D. Ma,[1] Jefferson Z. Liu,[2,*] Lifeng Wang,[3] Luming Shen,[4] Lin Xie,[5,6] Fei Wei,[7] Jing Zhu,[5,6] Qianming Gong,[8] Ji Liang,[8] and Quanshui Zheng[1,*]

[1]*Department of Engineering Mechanics, Tsinghua University, Beijing 100084, China*
[2]*Department of Mechanical and Aerospace Engineering, Monash University, Clayton, Victoria 3800, Australia*
[3]*Department of Mechanical Engineering, Massachusetts Institute of Technology, Cambridge, Massachusetts 02139, USA*
[4]*School of Civil Engineering, University of Sydney, Sydney, New South Wales 2006, Australia*
[5]*Beijing National Center for Electron Microscopy, Tsinghua University, Beijing 100084, China*
[6]*Laboratory of Advanced Materials, Department of Materials Science and Engineering, Tsinghua University, Beijing 100084, China*
[7]*Department of Chemical Engineering, Tsinghua University, Beijing 100084, China*
[8]*Department of Mechanical Engineering, Tsinghua University, Beijing 100084, China*

(Received 4 January 2010; revised manuscript received 29 March 2010; published 11 June 2010; corrected 30 July 2010)

Applying a full pressure loop, i.e., loading and unloading, on a nanocrystal with *in situ* observation remains a challenge to experimentalists up until now. Using a multiwalled carbon nanotube, we realize the pressure loop acting on a Fe_3C nanocrystal (with peak value 20 GPa) by electron-beam irradiation with *in situ* observations inside transmission electron microscopy at 500 °C/ambient temperature. Using density-functional theory calculations, we attribute the unloading process to the formation of one dangling-bond single vacancies under the electron-beam irradiation at room temperature. A theoretical model is presented to understand the process and the results agree well with the experimental measurements.

DOI: 10.1103/PhysRevB.81.235420 PACS number(s): 61.46.Fg, 62.25.−g, 61.80.Fe

I. INTRODUCTION

Studies into structural transformations in a nanocrystal are of great importance for understanding the microscopic mechanisms of the relevant solid-solid phase transition.[1] Pressure cycling plays an important role in investigating the hysteresis loop during such a transition.[1,2] For example, from the pressure dependence of relaxation time, which is obtained by using pressure cycling, Jacobs *et al.* determined the activation volume of CdSe nanocrystals.[1] The pressure required in these studies is usually as high as several GPa. Up to now, a diamond-anvil cell is still the best choice for a pressure vessel to study the structural transformation in nanocrystals because it can generate pressures above 100 GPa.[3] The inherent drawback of diamond-anvil cell settings, however, prohibits any *in situ* observation, which could provide enormous details of the structural change.[3] High-pressure transmission electron microscopy (TEM) is, meanwhile, the only analytical technique that can provide a visual image of the atomic structure in studying the structural transformations of nanocrystals.[3] Recently, Banhart and Ajayan found that carbon onions could build an internal pressure up to 36 GPa in its hollow vessel when exposed to electron beams at a temperature between 650 and 750 °C within a TEM.[4] A similar phenomenon was observed later in multiwalled carbon nanotubes (MWCNTs).[5] These two experiments with *in situ* observations have inspired using onions or MWCNTs as high-pressure vessels in studying pressure-induced structural transition and mechanical deformations of various solid nanosized crystals.[3,5,6] However, the unloading process at the other half of the pressure cycling has attracted much less attention. Up to now, the only observation of unloading process within carbon-nanostructures-based high-pressure vessels is made in carbon onions at temperature above 1500 °C.[7] So high an operating temperature severely limits its practical application, since it is higher than the melting points of many solids, such as Mg (650 °C), Al (660 °C), Ag (961 °C), Au (1,065 °C), CdSe (1268 °C), and Si (1,410 °C), let alone the even lower melting points of their corresponding nanocrystals. Therefore, a technique for conducting the unloading process at temperatures much lower than the typical melting points with *in situ* observations is highly desirable.

In this paper, we report an unloading process in MWCNT vessels at room temperature. This relaxation process is observed *in situ* in a TEM operated at 80 kV. Using density-functional theory (DFT) calculations, we attribute this unloading process to formation of one dangling-bond single vacancies under the electron-beam irradiation at room temperature.

II. EXPERIMENTAL DETAILS

The Fe_3C-filled samples were fabricated using the same method as described in Ref. 8. Figure 1(a) shows the TEM (JEOL 2011) image obtained at room temperature of an as-grown Fe_3C-filled MWCNT specimen. The experiments on this specimen were then carried out in two steps. During the first step, the specimen was irradiated at beam current density of 6 A/cm^2 for 19 min at 500 °C within a TEM (JEM 1000) operated at 750 kV. The electron beam was then turned off and the specimen was kept in the vacuum TEM chamber at 500 °C for 5 min before cooled down to the ambient temperature. The conditions used in our high-temperature irradiation are close to those used in Ref. 5.

In the second step, the irradiated and cooled-down specimen was put into another TEM (FEI Titan 80-300) operated at 80 kV, ambient temperature, and a current density around 100 A/cm^2. This specific acceleration voltage (80 kV) is proposed for the dual advantages of low damage rate and

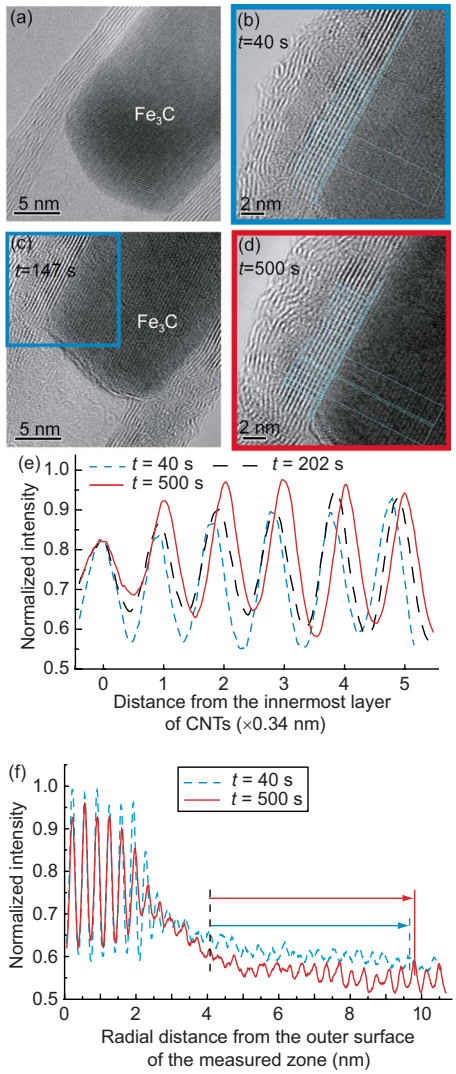

FIG. 1. (Color online) (a) TEM images of the as-grown Fe_3C-filled MWCNT and (b) the specimen which has been irradiated at 500 °C after exposed to electron-beam irradiation with acceleration voltage of 80 kV at room temperature for $t=40$ s, (c) 147 s, and (d) 500 s. [(e) and (f)] Typical gray scale intensity profiles of the labeled regions measured within MWCNTs only and both MWCNTs and Fe_3C. Labeled regions are shown in (b) and (d). Black (left) vertical dashed line in (f) represents the positions of certain crystal planes of the Fe_3C measured in (b) and (d) with the same radial distance from the outer surface of the measured zone and the gray (right) dashed-solid line in (f) represents the position of a certain crystal plane of the Fe_3C measured in (b) and (d), respectively. As the numbers of crystal planes between the black (left) vertical dashed line and the gray (right) dashed-solid line are the same, an expansion of the Fe_3C core is clear.

increased contrast due to a large atomic scattering factor.[9] The charge coupled device (CCD) of the TEM has 2048 $\times$2048 pixels and it was calibrated to the average interwall spacings of CNTs (0.34 nm) that are measured to be uniform for CNTs with diameters larger than 10 nm.[10] The precision (or absolute error) after calibration is 0.0084 nm. Figures 1(b)–1(d) show the TEM images of the same specimen that has been exposed to the electron beam for $t=40$, 147, and 500 s, respectively, with different magnifications. A multiscale zoom-in locating method is developed to trace the specimen during the whole experiment.[11] Comparison between Figs. 1(c) and 1(a) shows an 11.3% diameter shrinkage of the Fe_3C core, although a certain elastic relaxation has already occurred when the image was recorded (see text later). Figure 1(e) shows the typical gray scale intensity profiles of the labeled region in Fig. 1(b) at $t=40$ s (gray, dashed), in Fig. 1(d) at $t=500$ s (gray, solid), and in another image recorded at $t=202$ s (black, dashed), in which the peaks represent the positions of the solid walls. To make sure the sections of the MWCNT we measured before and after irradiation are exactly the same area, we first drew a reference line along the interface between the innermost layer of the MWCNT and the Fe_3C core [Figs. 1(b) and 1(d)]. Perpendicular to this line, we divided the MWCNT into several small strips with the same width. By selecting sections where the walls are straight both before and after irradiation, we were able to measure the interwall spacings within each section from the intensity profiles, which were obtained by integrating the gray intensity along the section. Figure 1(e) clearly shows relaxation of the MWCNT vessel under the electron-beam irradiation at room temperature: the interwall spacings measured at $t=40$ s from Fig. 1(e) among the innermost three layers are about 7% less than those among other layers, the difference drops to 4% at $t=202$ s, and all the interwall spacings measured after $t=500$ s become uniform 0.34 nm (i.e., the equilibrium spacing in the as-grown sample). The recovery process observed here is clearer if we take account of the *in situ* experiments of Sun *et al.*,[5] where after electron-beam irradiation at $T=600$ °C, the reduction of interlayer spacing is 10%–13% between the innermost two layers and 5% between the second and third walls. Since we were using the same material system and similar irradiation conditions, their results can be adopted as the reference state, i.e., $t=0$ s instantly after the irradiation of 500 °C, for our experiments. It is known that the distance-sensitive van der Waals interaction between the layers leads to interwall pressures.[5,12] The reduction and recovery of the interwall spacings of the MWCNT thus can serve as an indication of the pressure variation inside the vessel.[12]

The relaxation is also observed by directly measuring the lattice spacing in the encapsulated crystal. Although the TEM is not sensitive enough to detect the minute changes, the gray intensity profiles, as shown in Fig. 1(f), of the MWCNT and the Fe_3C crystal as highlighted in Figs. 1(b) and 1(d) still reveal a global 2.7% elastic expansion of the crystal from Fig. 1(b) to Fig. 1(d). It is noticeable that this pressure release is achieved at room temperature rather than at high temperatures, e.g., ~1500 °C in previous experiments.[7]

III. ATOMISTIC SIMULATIONS

Hereinafter, we are trying to gain an understanding of the above observations. Of MWCNTs, it is well known that the primary defects induced by electron-beam irradiation are mostly single vacancies (SVs) with one dangling bond and interstitials.[13–16] Since migration energy of interstitials in

MWCNTs with large diameters is close to that in graphene (0.1 eV),[17] they could migrate away from the contracting region where the pressure is high. So one can assume there are no interstitials in the irradiated region,[5] with only SVs left behind. At a temperature higher than 200 °C, these SVs become mobile and coalesce to form double vacancies (DVs).[18] Further atomistic simulations have revealed that the presence of DVs can result in significant radial shrinkage of single-walled carbon nanotubes (SWCNTs).[5] In this manner, the observed contracting phenomenon in Ref. 5 and in our experiment (in the first stage) can be well explained. The SVs, however, should be the most prolific defects in the second stage of our experiment which is conducted at ambient temperature. There have been no DFT simulations about the effects of SVs on the radius change and elastic mechanical properties of CNTs. The only reports about effects of SVs on the Young's modulus of SWCNTs were using empirical force field models[19,20] and these effects were significantly underestimated as will be shown by our DFT simulation detailed next.

We employed the density-functional theory calculations implemented in the Vienna *ab initio* simulation package (VASP) code[21] with generalized gradient approximation (GGA) approximation[22] adopted and performed the calculations with the ultrasoft pseudopotential. Electronic wave function is expanded by plane waves with cut off energy 400 eV. The Brillouin zone is sampled by employing the Monkhorst-Pack k-point meshes with a density ensuring the energy convergence within 1 meV/atom. The unit cells in our DFT simulations are (10,10) SWCNTs of about 1.3 nm long with periodic boundary conditions along the axial directions. In the radial direction, a supercell is used to ensure that there is no interaction between the CNT and its periodic images in the adjacent supercell (the nearest distance is kept ~2.5 nm). A SV is generated by removing one atom from a (10, 10) CNT and a DV is generated by removing two neighboring carbon atoms together and adjusting the adjacent atoms to form a prototype of DV similar to that shown in Ref. 18. Different levels of prescribed SVs or DVs are generated in the SWCNTs. The atomic structures are fully relaxed in our DFT simulations. The inset of Fig. 2(a) shows the relaxed SWCNT with a SV and that with a DV. The dots in Fig. 2(a) depict the effective radii of the fully relaxed SWCNT versus different contents of SVs or DVs. Nonorthogonal density-functional-theory-based tight-binding (DFTB) (Ref. 23) simulations are also performed for a wider range of DV concentration. These results [Fig. 2(a)] present almost a unified linear dependence (with dimensionless slope $k_1=-0.715$) of the effective radius upon knocked-off atom density, n, valid for both types of vacancies and for both simulation methods. The effects of SVs/DVs on the longitudinal Young's modulus are also calculated by applying a set of small uniaxial deformations on the fully relaxed defective SWCNT. The length of the supercell along the longitudinal direction is fixed while the internal atomic relaxation is allowed. Fitting the strain energy versus strain curve to a quadratic polynomial yields the Young's modulus. The linearity is also valid for the Young's modulus but with notably different dimensionless slopes, namely, $k_{2s}=-12.61$ for SVs and $k_{2d}=-7.54$ for DVs, as shown in Fig. 2(b). Note that the

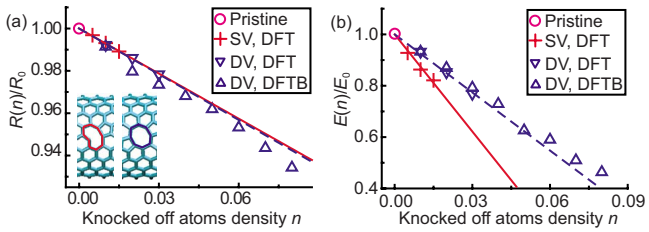

FIG. 2. (Color online) Effects of SVs and DVs on the (a) radius and (b) Young's modulus of a (10,10) SWCNT calculated with DFT and DFTB methods, where R_0(=0.68 nm) and E_0 (=1.03 or 1.18 TPa for DFT or DFTB) denote the radius and Young's modulus of the pristine (10,10) SWCNT. Solid and dashed straight lines are the least-squares fitting of the DFT results for SVs and DVs, respectively. The two fitted lines for the effective radius are almost identical, whereas those for Young's modulus are remarkably different. Inset in (a) shows the atomic networks of a (10,10) SWCNT with a typical 5–1 db SV (left) and a typical DV (right).

magnitude of the slope k_{2s} we obtained for a (10,10) SWCNT with SVs using DFT is 1.5 times higher than that obtained by using the empirical force field model (i.e., −8.45) for a (5,5) SWCNT.[20]

We note that the maximum knocked-off atom density is only 1.5% in our DFT simulations in the case of SVs. Beyond this density, we were not able to obtain convergent simulation results using either the DFT or DFTB method, probably due to presence of dangling bonds that are inherent in the SVs themselves [inset in Fig. 2(a)]. Fortunately, the linear dependences of the SWCNT's radius and Young's modulus on the SV density up to 6% are confirmed by additional molecular-dynamics (MD) simulations with an empirical force field model of second-generation reactive empirical bond order (REBO) with its extension.[24] We may, therefore, assume that the linear dependence shown in Fig. 2 would reasonably be valid for the concentration of SVs notably higher than 1.5%.

Now we are able to give a qualitative explanation why the unloading process could occur during the TEM observation conducted at room temperature. We consider a SWCNT stretched intrawall by an internal rigid bar. The intrawall stress of the SWCNT is proportional to the Young's modulus as well as the intrawall stretching strain. Note that an increase of knocked-off atom density will result in an increase of the intrawall stretching strain [Fig. 2(a)] as well as a decrease of the Young's modulus [Fig. 2(b)]. The overall effect may be an increase or a decrease of the intrawall stress, depending on tradeoff between the two mechanisms. If decrease of the Young's modulus dominates, the pressure between the SWCNT and the bar, which is proportional to the intrawall stress, becomes reduced.

IV. CONTINUUM MODEL

A quantitative continuum mechanics model based on the above explanation is proposed to explain the observed pressure relaxation of the studied MWCNT pressure vessel. We model each constituent wall of the MWCNT as an elastic shell. For a MWCNT with given knocked-off atomic density

n, the total energy of the system Π includes two parts: intrawall elastic energy density U_e and interwall van de Walls interaction energy density U_v,

$$\Pi = 2\pi s_0 \sum_{i=1}^{N} R_i U_e(\varepsilon_i^\theta, n) + \sum_{i=1}^{N-1} U_v(R_{i+1} - R_i), \quad (1)$$

where s_0 is the thickness of each single shell, N denotes the wall number, R_i is the equilibrium radius of the ith wall inside the irradiated MWCNT, $\varepsilon_i^\theta = R_i/R_i^s - 1$ is the circumferential strain of each shell, and R_i^s is the radius of the ith wall standing as an individual SWCNT with the knocked-off atom density n [Fig. 2(a)]. The bending energy of an individual shell is relatively small and thus neglected in our model.

To model the interwall van de Waals interactions, we replace the discrete distribution of atoms on each shell by a continuous distribution with the same atomic density. We note the use of the same approach by Henrard *et al.*[25] and Liu *et al.*[26] to calculate the intertube interaction potential for bundles of single-walled carbon nanotubes. The van de Waals energy can then be expressed as

$$U_v = \eta^2 \int \int 4\varepsilon[(\sigma/\rho)^{12} - (\sigma/\rho)^6] ds_i ds_{i+1}, \quad (2)$$

where ρ is the distance between the area element ds_i on ith wall and ds_{i+1} on $(i+1)$th wall and $\eta = 4\sqrt{3}/9a^2$ is the effective atomic density, where $a = 0.142$ nm is the carbon-carbon bond length. The integral of U_v is conducted using the same method as we proposed in our previous work.[27]

To model the elastic deformation within each shell of MWCNTs, we employ a linear elastic model

$$U_e(\varepsilon_i^\theta, n) = E(n)(\varepsilon_i^\theta)^2/2, \quad (3)$$

where $E(n)$ is the Young's modulus of a SWCNT with a knocked-off atomic density n. Here, we assume a linear addition of reductions in modulus E and reduction in radius R caused by the two different types of vacancies. Therefore, $E(n) = E_0(1 + k_{2s}n_1 + k_{2d}n_2)$, where n_1 is the knocked-off atomic density of SVs and n_2 is the knocked-off atomic density of DVs with $n_1 + n_2 = n$. Meanwhile, $R_i^s = (1 + k_1 n)R_i^0$, where R_i^s is the diameter of the ith wall as an individual SWCNT with the knocked-off atom density n and R_i^0 the diameter of this SWCNT as $n = 0$. The parameters, k_1, k_{2s}, and k_{2d}, are estimated by DFT simulations as shown in Fig. 2. Following practice in Ref. 5, we also assume that the DFT results calculated for the (10, 10) SWNT in Fig. 2 are applicable to nanotubes with any chiralities and diameters. Once n_1 and n_2 on each SWCNT in the MWCNT pressure vessel are known, we can solve R_i through minimizing Π. The pressure P between the Fe_3C core and the innermost layer of the MWCNT is then calculated as

$$P = s_0 \sum_{i=1}^{N} \sigma_i / R_i, \quad (4)$$

where $\sigma_i = E(n)\varepsilon_i^\theta$ is the in-plane elastic stress within each shell.

Figure 3(a) shows the pressure between the Fe_3C core and the innermost wall of the MWCNT, P, as a function of knocked-off atoms density n. The results to the left of the vertical dashed line at density $n \sim 8\%$ represent the first stage of our experiments at $T = 500$ °C. For a SWCNT, the pressure builds up with increase of DV density and then release starts at $n \approx 7\%$ [black solid curve in Fig. 3(a)], which is in accordance with our previous qualitative analysis, i.e., controlled by tradeoff between increase of the stretching strain and decrease of the elastic modulus. When a MWCNT is subjected to electron-beam irradiation at a temperature higher than 200 °C, the interwall spacing between its innermost two layers, d_{1-2}, decreases as the density of DVs increases [Fig. 3(b)] and reaches its minimum (around 10.5% reduction) at $n \approx 8\%$. The prediction of our model is consistent with the existing experimental observation, e.g., 10 ~ 13% reduction in d_{1-2} at $T = 600$ °C.[5] The predicted internal pressure is as high as ~20 GPa at $n \sim 8\%$. Maximum of the pressure increases with the number of layers in the MWCNT vessels and saturates when the number becomes relatively large, as demonstrated in Fig. 3(a).

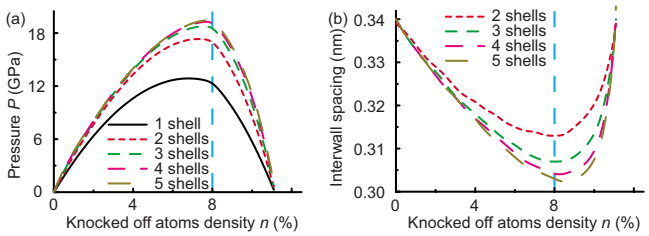

FIG. 3. (Color online) (a) Model predictions of the pressures P exerted on the Fe_3C core from the MWCNT vessels with different number of layers (as labeled) vs the knocked-off atom density n. (b) The model-predicted interwall spacings between the innermost two walls of the MWCNT extruders d_{1-2} with different layers (as labeled) vs n. Results to the left of the vertical dashed line account for DVs with knocked-off atoms density n from 0% to 8% and the results on the right-hand side account for the additional SVs with density from 0% to 3.1% as the DV density fixed at 8%.

Further irradiation at room temperature, as in the second stage of our experiments, introduces SVs and thus lead to expansion of the interwall spacing between the innermost two layers and release of the pressure exerted on the Fe_3C core due to the sharper decrease of the CNT's Young's modulus [Fig. 2(b)]. Those results are shown to the right of the vertical dashed lines in Figs. 3(a) and 3(b). Since the reduction of the interwall spacing of two innermost layer is measured as ~7% in our experiment [Fig. 1(e)], the corresponding defect density is $n_{SV} = 2.2\%$ in addition to $n_{DV} = 8\%$ as estimated from Fig. 3(b). The pressure acting on the Fe_3C core can thus be approximated as 10 GPa according to Fig. 3(a). By using compression modulus of Fe_3C (extrapolated from the Birth-Murnaghan equation[28]), a 1.7% expansion of Fe_3C lattice can be expected upon release of such a pressure, reasonably close to our measured value of ~2.7%.

Based on the atom displacement rate relation,[16] the maximal defect density n_{max} can be estimated as $n_{max} = sjt$, where s is the displacement cross section, j beam current density, and t irradiation time. For radiating CNTs within TEM operated at 80 kV, a displacement cross section of $s = 3$ barn could be estimated by applying the McKinley-Feshbach

formalism[29] and a displacement threshold energy of $T_d = 15$ eV assumed, which might be realistic for a relatively large tube.[30] With $j = 100$ A/cm^2, we obtained $n_{max} = 3\%$ for SV after just 15 s room-temperature irradiation, which indicates that d_{1-2} will recover to its normal value (~0.34 nm) according to Fig. 3(b). Note that the actual defect concentrations may be 1 order of magnitude lower than n_{max} due to immediate recombination of vacancy-interstitial pairs[13] and the time required to release the internal pressure will become longer accordingly, agreeing reasonably well with our observation, about 4–8 min. Whereas under electron-beam irradiation with an acceleration voltage of 200 kV, which is usually adopted in TEM, at room temperature, the interwall spacing is predicted to recover to its normal value (~0.34 nm) within only a few seconds. This prediction has also been supported by our experiments conducted within a TEM with an acceleration voltage 200 kV, at room temperature, where no compression was observed.

V. SUMMARY

In summary, we report in this paper an unloading process in multiwalled carbon nanotube-based, high-pressure vessels at room temperature with an *in situ* observation. Using DFT computations together with a continuum model, we show that the one-dangling-bond single vacancies generated by electron-beam irradiation at room temperature play a crucial role during this unloading process. The significant reduction in elastic modulus caused by single vacancies leads to weakening of the pressure sustainability and thus release of the pressure. By analogy with the work described in Ref. 5, our experiment suggests an avenue to use carbon nanotubes as reversible high-pressure nanovessels at moderate temperature (500 °C) with *in situ* observations in investigating structural transition as well as other pressure-sensitive properties of nanocrystals.

ACKNOWLEDGMENTS

The authors thank Jiguang Sun and Tongda Ma (HVEM lab, General Research Institute for Nonferrous Metals, Beijing) for their support on electron irradiation in HVEM.

*Corresponding authors; jzliu@eng.monash.edu.au; zhengqs@tsinghua.edu.cn

[1] K. Jacobs, D. Zaziski, E. C. Scher, A. B. Herhold, and A. P. Alivisatos, Science **293**, 1803 (2001).
[2] K. J. Koski, N. M. Kamp, R. K. Smith, M. Kunz, J. K. Knight, and A. P. Alivisatos, Phys. Rev. B **78**, 165410 (2008).
[3] Z. W. Wang and Y. S. Zhao, Science **312**, 1149 (2006).
[4] F. Banhart and P. M. Ajayan, Nature (London) **382**, 433 (1996).
[5] L. Sun, F. Banhart, A. V. Krasheninnikov, J. A. Rodriguez-Manzo, M. Terrones, and P. M. Ajayan, Science **312**, 1199 (2006).
[6] J. X. Li and F. Banhart, Adv. Mater. **17**, 1539 (2005).
[7] Y. J. Gan and F. Banhart, Adv. Mater. **20**, 4751 (2008).
[8] X. C. Gui, J. Q. Wei, K. L. Wang, W. Wang, R. Lv, J. Chang, F. Kang, J. Gu, and D. Wu, Mater. Res. Bull. **43**, 3441 (2008).
[9] B. W. Smith and D. E. Luzzi, J. Appl. Phys. **90**, 3509 (2001).
[10] C. H. Kiang, M. Endo, P. M. Ajayan, G. Dresselhaus, and M. S. Dresselhaus, Phys. Rev. Lett. **81**, 1869 (1998).
[11] See supplementary material at http://link.aps.org/supplemental/10.1103/PhysRevB.81.235420 for more details of the specimen locating method.
[12] Z. P. Xu, L. F. Wang, and Q. S. Zheng, Small **4**, 733 (2008).
[13] A. V. Krasheninnikov and F. Banhart, Nat. Mater. **6**, 723 (2007).
[14] J. Kotakoski, A. V. Krasheninnikov, and K. Nordlund, Phys. Rev. B **74**, 245420 (2006).
[15] A. A. El-Barbary, R. H. Telling, C. P. Ewels, M. I. Heggie, and P. R. Briddon, Phys. Rev. B **68**, 144107 (2003).
[16] F. Banhart, Rep. Prog. Phys. **62**, 1181 (1999).
[17] A. V. Krasheninnikov, K. Nordlund, P. O. Lehtinen, A. S. Foster, A. Ayuela, and R. M. Nieminen, Phys. Rev. B **69**, 073402 (2004).
[18] A. V. Krasheninnikov, P. O. Lehtinen, A. S. Foster, and R. M. Nieminen, Chem. Phys. Lett. **418**, 132 (2006).
[19] S. L. Zhang, S. L. Mielke, R. Khare, D. Troya, R. S. Ruoff, G. C. Schatz, and T. Belytschko, Phys. Rev. B **71**, 115403 (2005).
[20] M. Sammalkorpi, A. Krasheninnikov, A. Kuronen, K. Nordlund, and K. Kaski, Phys. Rev. B **70**, 245416 (2004).
[21] G. Kresse and J. Furthmuller, Phys. Rev. B **54**, 11169 (1996).
[22] J. P. Perdew, J. A. Chevary, S. H. Vosko, K. A. Jackson, M. R. Pederson, D. J. Singh, and C. Fiolhais, Phys. Rev. B **46**, 6671 (1992).
[23] T. Frauenheim *et al.*, J. Phys.: Condens. Matter **14**, 3015 (2002).
[24] S. J. Stuart, A. B. Tutein, and J. A. Harrison, J. Chem. Phys. **112**, 6472 (2000).
[25] L. Henrard, E. Hernandez, P. Bernier, and A. Rubio, Phys. Rev. B **60**, R8521 (1999).
[26] J. Z. Liu, Q. S. Zheng, L. F. Wang, and Q. Jiang, J. Mech. Phys. Solids **53**, 123 (2005).
[27] Q. Zheng, J. Z. Liu, and Q. Jiang, Phys. Rev. B **65**, 245409 (2002).
[28] J. Li, H. K. Mao, Y. Fei, E. Gregoryanz, M. Eremets, and C. S. Zha, Phys. Chem. Miner. **29**, 166 (2002).
[29] W. A. McKinley and H. Feshbach, Phys. Rev. **74**, 1759 (1948).
[30] F. Banhart, J. X. Li, and A. V. Krasheninnikov, Phys. Rev. B **71**, 241408(R) (2005).